Conditional transgenic expression of fibroblast growth factor 9 in the adult mouse heart reduces heart failure mortality after myocardial infarction

Conditional Transgenic Expression of Fibroblast Growth Factor 9 in the Adult Mouse Heart Reduces Heart Failure Mortality After Myocardial Infarction

Mortimer Korf-Klingebiel, Tibor Kempf, Klaus-Dieter Schlüter, Christian Willenbockel, Torben Brod, Jörg Heineke, Volker J. Schmidt, Franziska Jantzen, Ralf P. Brandes, Peter H. Sugden, Helmut Drexler, Jeffery D. Molkentin and Kai C. Wollert

Circulation. 2011;123:504-514; originally published online January 24, 2011;
doi: 10.1161/CIRCULATIONAHA.110.989665
Circulation is published by the American Heart Association, 7272 Greenville Avenue, Dallas, TX 75231

Print ISSN: 0009-7322. Online ISSN: 1524-4539

Conditional Transgenic Expression of Fibroblast Growth Factor 9 in the Adult Mouse Heart Reduces Heart Failure Mortality After Myocardial Infarction

Mortimer Korf-Klingebiel, PhD; Tibor Kempf, MD; Klaus-Dieter Schlüter, MD; Christian Willenbockel, DVM; Torben Brod, BS; Jörg Heineke, MD; Volker J. Schmidt, MD; Franziska Jantzen, PhD; Ralf P. Brandes, MD; Peter H. Sugden, PhD; Helmut Drexler, MD;† Jeffery D. Molkentin, PhD; Kai C. Wollert, MD

Background—Fibroblast growth factor 9 (FGF9) is secreted from bone marrow cells, which have been shown to improve systolic function after myocardial infarction (MI) in a clinical trial. FGF9 promotes cardiac vascularization during embryonic development but is only weakly expressed in the adult heart.

Methods and Results—We used a tetracycline-responsive binary transgene system based on the α-myosin heavy chain promoter to test whether conditional expression of FGF9 in the adult myocardium supports adaptation after MI. In sham-operated mice, transgenic FGF9 stimulated left ventricular hypertrophy with microvessel expansion and preserved systolic and diastolic function. After coronary artery ligation, transgenic FGF9 enhanced hypertrophy of the noninfarcted left ventricular myocardium with increased microvessel density, reduced interstitial fibrosis, attenuated fetal gene expression, and improved systolic function. Heart failure mortality after MI was markedly reduced by transgenic FGF9, whereas rupture rates were not affected. Adenoviral FGF9 gene transfer after MI similarly promoted left ventricular hypertrophy with improved systolic function and reduced heart failure mortality. Mechanistically, FGF9 stimulated proliferation and network formation of endothelial cells but induced no direct hypertrophic effects in neonatal or adult rat cardiomyocytes in vitro. FGF9-stimulated endothelial cell supernatants, however, induced cardiomyocyte hypertrophy via paracrine release of bone morphogenetic protein 6. In accord with this observation, expression of bone morphogenetic protein 6 and phosphorylation of its downstream targets SMAD1/5 were increased in the myocardium of FGF9 transgenic mice.

Conclusions—Conditional expression of FGF9 promotes myocardial vascularization and hypertrophy with enhanced systolic function and reduced heart failure mortality after MI. These observations suggest a previously unrecognized therapeutic potential for FGF9 after MI. (***Circulation*. 2011;123:504-514.**)

Key Words: angiogenesis ■ cardiac remodeling ■ FGF9 ■ mortality ■ myocardial infarction

Advances in treatment have resulted in declining mortality rates after acute myocardial infarction (MI). Unfortunately, the decrease in postinfarct mortality is paralleled by an increase in the incidence of heart failure in patients surviving with significant residual myocardial damage.[1] Loss of contractile tissue after MI induces profound alterations of left ventricular (LV) tissue architecture that are characterized by chamber dilatation and pathological hypertrophy of the noninfarcted myocardium, leading to contractile dysfunction and reduced long-term survival.[2]

Clinical Perspective on p 514

During midgestational heart development, the heart undergoes a dramatic increase in size that is attributable to cardiomyoblast proliferation and the concurrent formation of the coronary vascular system.[3,4] LV contractile function increases during this period of rapid cardiac growth,[5] thus providing an example that cardiac mass and size can increase considerably without deleterious effects on systolic function or lifespan. Fibroblast growth factor (FGF) 9 acts as an

Received April 1, 2010; accepted November 23, 2010.

From the Hans-Borst-Center for Heart and Stem Cell Research, Department of Cardiology and Angiology, Hannover Medical School, Hannover, Germany (M.K.K., T.K., C.W., T.B., J.H., V.J.S., F.J., H.D., K.C.W.); Institute of Physiology, Justus-Liebig-University, Gießen, Germany (K.D.S.); Institute of Cardiovascular Physiology, Johann-Wolfgang-Goethe-University, Frankfurt am Main, Germany (R.P.B.); Institute for Cardiovascular and Metabolic Research, University of Reading, Reading, UK (P.H.S.); and Division of Molecular Cardiovascular Biology and Howard Hughes Medical Institute, University of Cincinnati, Cincinnati Children's Hospital Medical Center, Ohio (J.H., J.D.M.).

†Deceased.

The online-only Data Supplement is available with this article at http://circ.ahajournals.org/cgi/content/full/CIRCULATIONAHA.110. 989665/DC1.

Correspondence to Kai C. Wollert, Department of Cardiology and Angiology, Hannover Medical School, Carl-Neuberg-Straße 1, 30625 Hannover, Germany. E-mail wollert.kai@mh-hannover.de

Circulation **is available at http://circ.ahajournals.org** **DOI: 10.1161/CIRCULATIONAHA.110.989665**

essential inducer of midgestational cardiac growth and vascularization.[6,7]

FGF9 is a member of the FGF gene family, which comprises 22 functionally diverse polypeptides in humans and mice that can be divided into subfamilies based on their chromosomal location and evolutionary relationships, their function as intracellular or secreted proteins, and their biochemical properties.[8] FGF9 acts as a secreted factor and exerts its functions via transmembrane FGF receptors on target cells.[8,9] Because of its affinity for pericellular heparan sulfate proteoglycans, FGF9 diffuses locally within tissues and acts primarily in a paracrine fashion.[10] During midgestation, FGF9 is expressed by the epicardium and endocardium and provides an epithelial-to-mesenchymal signal to stimulate coronary artery formation and cardiomyoblast expansion in the developing myocardium.[6,7] FGF9 is expressed only at low levels in the adult heart,[11] and previous transcriptome analyses provided no evidence for a reinduction of FGF9 expression after MI.[12]

We have recently shown that FGF9 is secreted from bone marrow cells (BMCs) that we have found in a randomized controlled cell therapy trial to enhance the recovery of LV ejection fraction in patients after MI.[13,14] Paracrine mechanisms are thought to contribute to the beneficial effects of BMCs on perfusion and function of the infarcted heart that have been demonstrated in experimental studies and some clinical trials.[15,16] Considering the pivotal role of FGF9 in supporting cardiac growth and vascularization during development, we therefore hypothesized that increased expression levels of FGF9 may help the heart adapt to a MI. Our data indicate that conditional transgenic expression of FGF9 in the adult mouse myocardium promotes adaptive LV hypertrophy with enhanced systolic function and reduced heart failure mortality after MI, thus pointing to FGF9 as a potential therapeutic strategy after MI.

Methods

An expanded Methods section is provided in the online-only Data Supplement.

Mouse and rat cells were stimulated with recombinant mouse FGF9 and bone morphogenetic protein 6 (BMP6), human cells with recombinant human FGF9. Dorsomorphin was used as an inhibitor of activin receptor-like kinase (ALK) 2, ALK3, and ALK6.[17] SB-431542 was used as an inhibitor of ALK4, ALK5, and ALK7.[18]

A tetracycline-responsive transgene system[19] was used to allow temporally regulated expression of FGF9 in adult cardiac myocytes. Mouse FGF9 cDNA was placed under the chimeric tetracycline-responsive α-myosin heavy chain (MHC) promoter (responder mice). FGF9 transgenic mice were crossed with transgenic mice expressing the tetracycline transactivator (tTA) under the control of the constitutive αMHC promoter. All mice were generated and bred on an FVB/N background. Doxycycline was provided in the drinking water from mating up to 8 weeks after birth to inhibit FGF9 transgene expression; doxycycline was then withdrawn to induce FGF9 expression.

MI was induced in male mice by permanent left anterior descending coronary artery (LAD) ligation during isoflurane anesthesia. A sham operation was performed in control mice. Mice were followed up and inspected daily from 24 hours up to 6 weeks after MI. Autopsies were performed on all dead animals; rupture was diagnosed by the presence of a blood clot around the heart and in the chest cavity; heart failure was diagnosed by chest fluid accumulation.[20,21]

Replication-deficient adenoviruses encoding mouse FGF9 (Ad.FGF9) or β-galactosidase (Ad.lacZ) were injected into the LV cavity immediately after LAD ligation.

Steady-state LV pressure-volume loops were recorded with a 1.4F micromanometer conductance catheter (SPR-839, Millar Instruments, Houston, TX) inserted via the right carotid artery during isoflurane anesthesia. Transthoracic echocardiography was performed with a linear 30-MHz transducer in mice sedated with isoflurane.

Infarct sizes were determined in paraffin-embedded tissue sections stained with Masson trichrome. Infarct sizes were calculated as the average ratio of endocardial scar length to endocardial total LV circumference in basal, midventricular, and apical sections. Scar thickness was measured at the center of the infarct in the same sections. Midventricular cryosections were prepared for fluorescent (immuno)staining. Cardiomyocytes were outlined by TRITC-conjugated wheat germ agglutinin (WGA). The circumferences of 40 to 50 myocytes were traced and digitized to calculate mean cardiomyocyte cross-sectional area. Ki67 was detected with a rabbit polyclonal antibody; troponin T, with a mouse monoclonal antibody. Capillaries were stained with fluorescein-labeled GSL I-isolectin B4. Conductance vessels were identified by their diameter (>20 μm) after immunostaining for smooth muscle α-smooth muscle actin (αSMA). Interstitial collagen content was determined by Picrosirius Red polarization microscopy.

Cardiac gene expression levels were quantified by quantitative polymerase chain reaction (polymerase chain reaction primers are shown in Table I in the online-only Data Supplement).

Human coronary artery endothelial cells (HCAECs) were purchased from Provitro (Berlin, Germany). Primary mouse heart endothelial cells were isolated as previously described.[22] Endothelial cell proliferation was measured by bromodeoxyuridine incorporation. Network formation was assayed in tissue culture plates coated with growth factor–reduced Matrigel. Ventricular cardiomyocytes were isolated from 1- to 3-day-old Sprague-Dawley rats by Percoll density gradient centrifugation. Cell size was determined by planimetry; protein content was assessed by the Bradford assay. Adult ventricular cardiomyocytes were isolated from 4-month-old Wistar rats. Cross-sectional area of adult cardiomyocytes was calculated as follows: $(\text{cell width}/2)^2 \times \pi$. Net protein synthesis was measured by [^{14}C] phenylalanine incorporation.

Antibodies against mouse FGF9, BMP6, phospho-SMAD1/5, phospho-SMAD3, and β-actin were used for immunoblotting. Expression levels of 174 secreted factors were assessed in conditioned HCAEC supernatants with Human Cytokine ProteinChip Array C Series 2000 membranes (Ray Biotech, Norcross, GA).

Statistical Analysis

Data are presented as mean±SEM. The unpaired t test was used for comparisons between 2 groups. For comparisons between >2 groups, we used 1-way ANOVA if there was 1 independent variable and 2-way ANOVA if there were 2 independent variables (ie, genotype and LAD ligation status). The Tukey posthoc test was used to adjust for multiple comparisons. Pairwise comparisons were made between sham groups across genotypes, sham versus MI within each genotype, and MI groups across genotypes. Kaplan–Meier curves were created to illustrate cumulative mortality after MI, and statistical assessment was performed by the log-rank test. A 2-tailed value of $P<0.05$ was considered to indicate statistical significance.

Results

Generation of Inducible, Cardiac-Specific FGF9 Transgenic Mice

Inducible and heart-specific expression of FGF9 was achieved with a binary αMHC promoter-based transgene

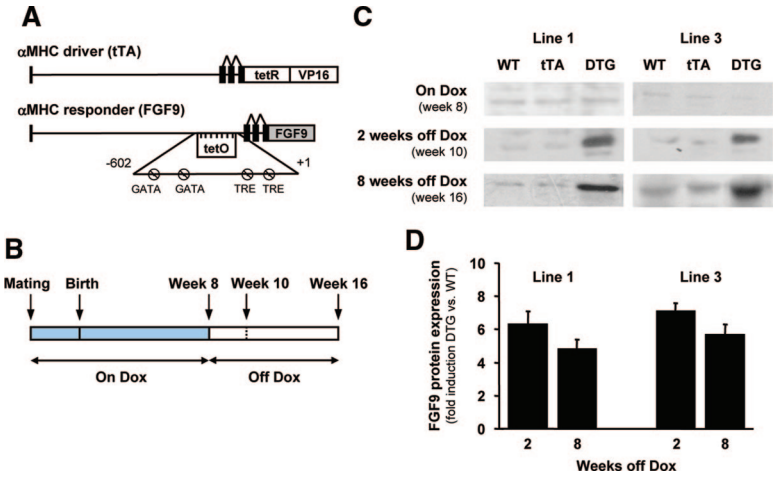

Figure 1. Inducible, cardiac-specific FGF9 transgenic mice. A, Schematic representation of the binary transgene system. B, Time schedule of doxycycline (Dox) treatment and FGF9 transgene expression (blue, FGF9 not expressed; white, FGF9 expressed). C, Immunoblots showing FGF9 expression in the LV myocardium at 8 weeks of age (mice still on Dox) and at 10 and 16 weeks of age (mice off Dox for 2 or 8 weeks) in WT, tTA single transgenic, and tTA/FGF9 DTG mice from lines 1 and 3. D, Quantification of FGF9 protein expression (8 to 10 animals per group).

strategy (Figure 1A). Two independent responder transgenic lines were generated (lines 1 and 3). Each permitted expression of FGF9 in the heart only in the presence of the driver transgene encoding the tTA when doxycycline was absent. In all experiments, doxycycline was administered from mating up to 8 weeks after birth, which blocks developmental expression, followed by doxycycline withdrawal thereafter to permit transgene expression starting in young adulthood (Figure 1B). In tTA/FGF9 double transgenic (DTG) mice from line 1, LV FGF9 protein expression was increased 6.3-fold at 2 weeks and 4.8-fold at 8 weeks after doxycycline withdrawal compared with wild-type (WT) mice (Figure 1C and 1D). A similar degree of FGF9 induction was observed in line 3 (Figure 1C and 1D). Data from line 1 are presented here. Line 3 displayed an identical cardiac phenotype (not shown).

FGF9 Promotes Cardiac Hypertrophy

To assess the effects of prolonged FGF9 expression on the adult unstressed myocardium, mice were followed up for up to 8 weeks after doxycycline withdrawal. Mice underwent a sham operation 2 weeks after doxycycline removal to allow comparison with mice undergoing LAD ligation at this time point (see below). No increase in LV mass was apparent at 2 weeks, but after 8 weeks of doxycycline withdrawal, LV mass (Figure 2A) and the ratio of LV mass to body mass (Figure 2B) were increased in DTG compared with WT and tTA control mice. No differences in body weight were observed between the genotypes (not shown). The increases in LV mass and heart size (Figure 2C) in DTG mice were related to an increase in LV wall thickness with no apparent increase in LV cavity diameter (Figure 2D). On histological examination, DTG mice displayed a significant increase in

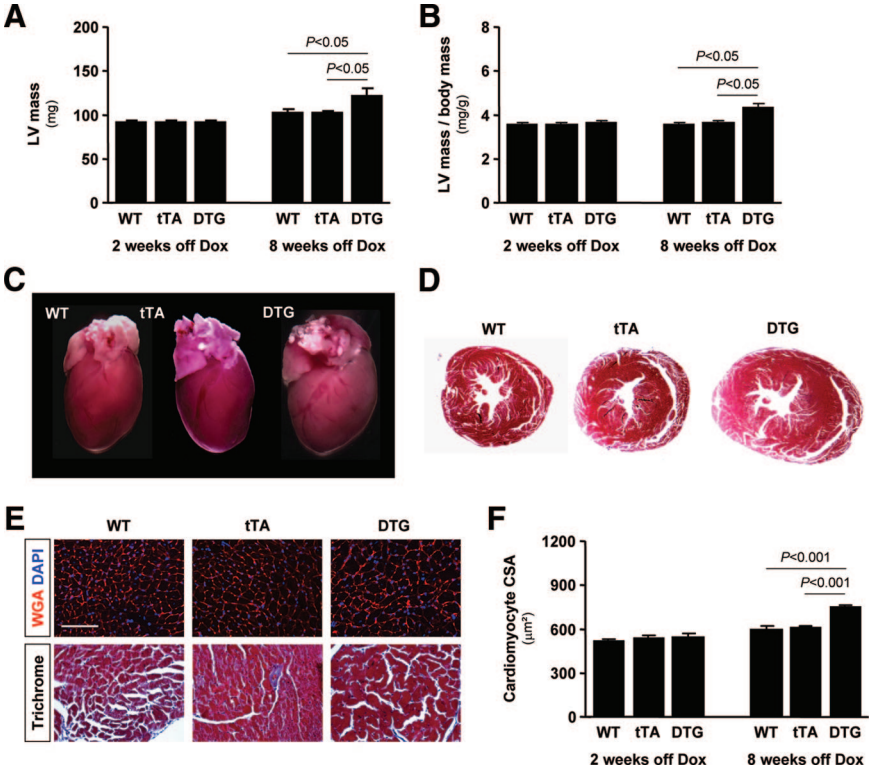

Figure 2. FGF9 promotes cardiac hypertrophy. LV mass (A) and ratio of LV mass to body mass (B) in WT, tTA single transgenic, and tTA/FGF9 DTG mice 2 and 8 weeks after doxycycline (Dox) withdrawal. Hearts (C) and transverse heart sections (D) stained with Masson trichrome 8 weeks after Dox withdrawal. E, LV tissue sections stained with WGA and DAPI or Masson trichrome 8 weeks after Dox removal (scale bar, 100 μm). F, Mean LV cardiomyocyte cross-sectional area (CSA) 2 and 8 weeks after Dox withdrawal; 8 animals per group in A, B, and F.

LV cardiomyocyte cross-sectional area 8 weeks after doxycycline withdrawal compared with WT and tTA controls (Figure 2E and 2F). Expression of transcripts of atrial natriuretic peptide, αMHC, βMHC, sarco(endo)plasmic reticulum Ca^{2+} ATPase 2a (SERCA2a), and phospholamban was not significantly different between WT, tTA, and DTG mice (Table II in the online-only Data Supplement, sham).

No differences in tail-cuff blood pressure or heart rate were observed between the 3 genotypes after 8 weeks of doxycycline treatment or during 8 weeks after doxycycline withdrawal (Figure I in the online-only Data Supplement, sham). Eight weeks after doxycycline withdrawal, invasive pressure-volume measurements revealed no significant differences between the 3 genotypes with regard to LV end-diastolic or end-systolic volumes and several indexes of systolic and diastolic function (Table 1, sham). Typical pressure-volume loops are shown in Figure II in the online-only Data Supplement. On 2-dimensional echocardiography, DTG mice displayed an increase in LV posterior wall thickness, normal internal LV dimensions, and preserved systolic function (Table III in the online-only Data Supplement, sham).

Table 1. Invasive Pressure-Volume Measurements 6 Weeks After Sham Operation or LAD Ligation

	WT	tTA	DTG
Sham, n	5	6	6
Heart rate, bpm	541±16	530±24	499±16
LV end-systolic volume, μL	11±1	13±3	13±2
LV end-diastolic volume, μL	32±3	32±3	35±3
LV end-systolic pressure, mm Hg	79±5	85±7	84±3
LV end-diastolic pressure, mm Hg	7±1	9±2	9±1
Ejection fraction, %	71±4	68±6	68±2
Cardiac output, μL/min	12595±1677	11760±544	12371±689
Stroke work, mm Hg×μL	1861±310	1884±177	2055±143
dP/dtmax, mm Hg/s	11464±904	10615±745	10448±1120
dP/dtmin, mm Hg/s	−7126±392	−7985±472	−8331±353
τ w, ms	6.5±0.4	6.4±0.4	6.4±0.4
LAD ligation, n	10	11	13
Heart rate, bpm	489±17	512±6	496±13
LV end-systolic volume, μL	39±4‡	40±3‡	27±3†§¶
LV end-diastolic volume, μL	49±3*	50±3†	41±3
LV end-systolic pressure, mm Hg	81±3	75±3	84±4
LV end-diastolic pressure, mm Hg	10±2	7±1	8±1
Ejection fraction, %	27±3‡	26±2‡	43±3‡‖#
Cardiac output, μL/min	6316±385‡	6501±387†	8915±738*§¶
Stroke work, mm Hg×μL	844±147†	690±48‡	1260±123†§#
dP/dtmax, mm Hg/s	6027±494†	6024±318‡	7828±376‖#
dP/dtmin, mm Hg/s	−4750±399†	−4857±274†	−5756±239‡
τ w, ms	10.3±1.0†	8.7±0.5†	8.5±0.6*

WT, tTA single transgenic, and tTA/FGF9 DTG mice were treated with doxycycline from mating until 8 weeks after birth. Doxycycline was then withdrawn. Mice underwent a sham operation or LAD ligation 2 weeks after doxycycline withdrawal. Hemodynamic measurements were performed 6 weeks later.

*$P<0.05$, †$P<0.01$, ‡$P<0.001$ versus same genotype sham; §$P<0.05$, ‖$P<0.01$ versus WT LAD ligation; ¶$P<0.05$, #$P<0.01$ versus tTA LAD ligation.

FGF9 Enhances Microvessel Density in the Myocardium

Two weeks after doxycycline withdrawal, the density of proliferating, $Ki67^+$ isolectin $B4^+$ endothelial cells was increased in the LV myocardium of DTG mice (Figure 3A and 3B). Eight weeks after doxycycline withdrawal, $Ki67^+$ endothelial cell density remained elevated in DTG mice and was accompanied by an increase in capillary density (Figure 3A and 3C) and an increase in the density of small (20 to 50 μm in diameter) αSMA^+ conductance vessels (Figure 3A and 3D). Two and 8 weeks after doxycycline withdrawal, no $Ki67^+$ cardiomyocyte nuclei were detectable in multiple tissue sections stained with anti-Ki67 and anti–troponin T antibodies and DAPI (not shown).

Eight weeks after doxycycline withdrawal, no significant differences emerged between the genotypes (4 to 6 mice per group) in the density of larger (>50 μm) αSMA^+ vessels (WT, 0.38±0.13; tTA, 0.40±0.06; DTG, 0.33±0.05 vessels per 100 cardiomyocytes) and interstitial collagen volume fraction in the LV myocardium (WT, 0.17±0.01%; tTA, 0.16±0.01%; DTG, 0.17±0.01%).

FGF9 Stimulates Endothelial Cell Proliferation, Network Formation, and Release of Prohypertrophic Factor(s)

Cardiomyocyte hypertrophy and microvessel expansion represented the main phenotypes observed in FGF9-expressing DTG mice. To explore whether FGF9 has a direct effect on cardiomyocyte hypertrophy, we stimulated neonatal cardiomyocytes with increasing concentrations of FGF9. Only at high concentrations (≥100 ng/mL) did FGF9 promote an increase in cardiomyocyte size, which was, however, much less pronounced than the response to endothelin 1 that we used as a positive control (Figure 4A). FGF9 did not promote a significant increase in cardiomyocyte protein content, which was chosen as an additional readout of hypertrophy (Figure III in the online-only Data Supplement).

Although cardiomyocytes were only weakly responsive to FGF9, HCAECs responded to markedly lower concentrations (≤10 ng/mL) of FGF9 with proliferation (Figure 4B) and network formation (Figure 4C and 4D). The effects of FGF9 on HCAECs were at least as potent as the effects of vascular endothelial growth factor, which we used as positive control.

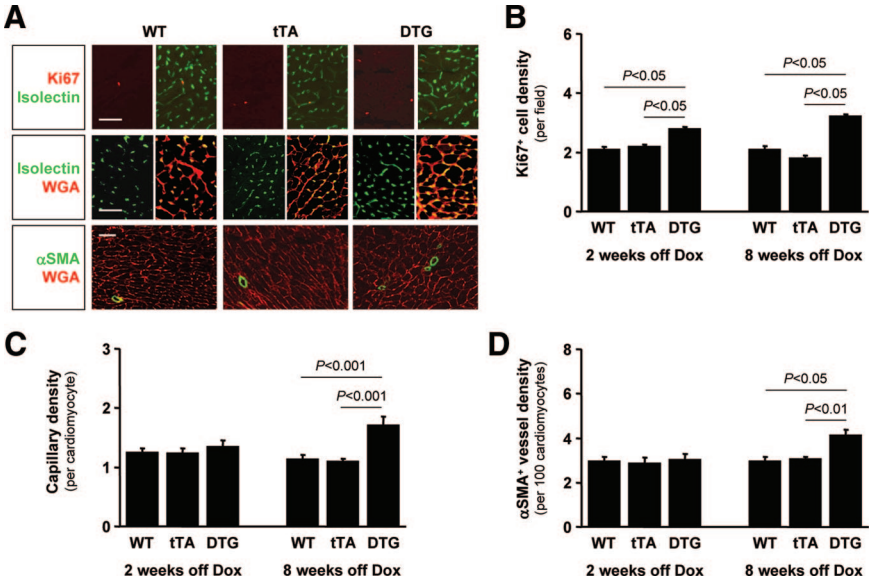

Figure 3. FGF9 enhances microvessel density in the myocardium. A, LV tissue sections from WT, tTA single transgenic, and tTA/FGF9 DTG mice stained with anti-Ki67 antibody and isolectin B4 to detect proliferating endothelial cells (top row), with isolectin B4 to detect capillaries (cardiomyocyte borders highlighted by WGA staining; middle row), and with anti-αSMA antibody to detect conductance vessels (cardiomyocyte borders highlighted by WGA staining; bottom row) 8 weeks after doxycycline (Dox) withdrawal (scale bars, 50 μm). Quantification of $Ki67^+$ isolectin $B4^+$ cell density (B), capillary density (C), and conductance vessel (D; 20 to 50 μm) density in LV myocardium 2 and 8 weeks after Dox withdrawal (4 to 6 animals per group).

These data led us to hypothesize that FGF9 induces cardiomyocyte hypertrophy by stimulating endothelial cells to release prohypertrophic factor(s). Indeed, conditioned supernatants from HCAECs stimulated for 24 hours with 10 ng/mL FGF9 promoted a significant increase in cardiomyocyte size, whereas conditioned supernatants from unstimulated HCAECs did not (Figure 4E and 4F). Similar results were obtained when protein content was used as a readout of hypertrophy (Figure 4G).

BMP6 Is Induced by FGF9 In Vitro and In Vivo and Stimulates Cardiomyocyte Hypertrophy

An antibody array detecting 174 cytokines, chemokines, and growth factors was used to identify factors secreted from HCAECs stimulated with 10 ng/mL FGF9 for 24 hours. Nine secreted factors were induced ≥2-fold by FGF9 in 2 independent array analyses (Table IV in the online-only Data Supplement). BMP6 was induced 2.5-fold and 6.8-fold in the 2 experiments, and its average increase was greater than for any other factor.

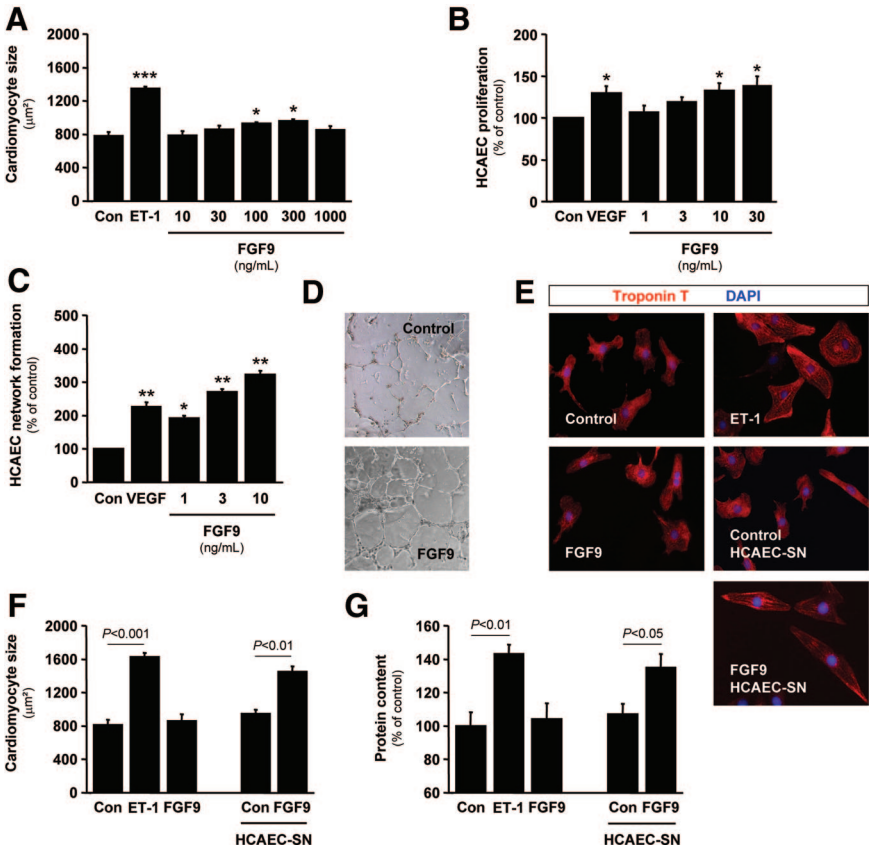

Figure 4. FGF9 stimulates endothelial cell proliferation, network formation, and release of prohypertrophic factor(s). A, Cell size of neonatal cardiomyocytes stimulated for 24 hours with 100 nmol/L endothelin 1 (ET1) or increasing concentrations of FGF9 (3 experiments; $^*P<0.05$, $^{***}P<0.001$ vs control). Proliferation (B) and network formation (C) of HCAECs stimulated for 24 hours with 10 ng/mL vascular endothelial growth factor (VEGF) or increasing concentrations of FGF9 (3 to 5 experiments; $^*P<0.05$, $^{**}P<0.01$ vs control). D, Images of HCAECs under control conditions and after stimulation with 10 ng/mL FGF9. E, Images of neonatal cardiomyocytes kept for 24 hours under control conditions or stimulated with 100 nmol/L ET1, 10 ng/mL FGF9, supernatant (1:2 dilution) obtained from HCAECs kept for 24 hours in serum-free medium (control HCAEC-SN), or supernatant (1:2 dilution) obtained from HCAECs stimulated for 24 hours with 10 ng/mL FGF9 (FGF9 HCAEC-SN); cells were stained with an anti–troponin T antibody and DAPI. Cell size (F) and protein content (G) of neonatal cardiomyocytes kept for 24 hours under the conditions described in E (4 to 6 experiments).

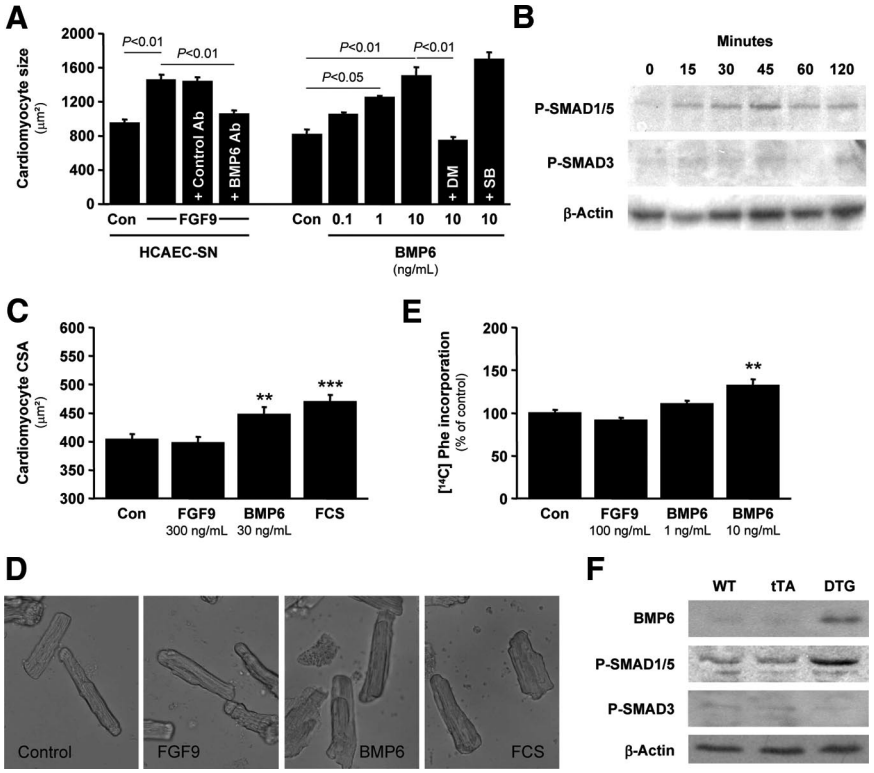

Figure 5. BMP6 is induced by FGF9 in vitro and in vivo and stimulates cardiomyocyte hypertrophy. A, Cell size of neonatal cardiomyocytes stimulated for 24 hours with supernatant (1:2 dilution) obtained from HCAECs kept for 24 hours in serum-free medium or stimulated for 24 hours with 10 ng/mL FGF9 (control and FGF9 HCAEC-SN). When indicated, a BMP6-neutralizing antibody or control antibody (20 μg/mL each) was added to the FGF9 HCAEC-SN. Cardiomyocytes were also stimulated with increasing concentrations of BMP6 in the presence or absence of the ALK2/3/6 inhibitor dorsomorphin (DM; 20 μmol/L) or the ALK4/5/7 inhibitor SB-431542 (SB; 20 μmol/L) (3 experiments). B, Immunoblot analysis of phospho-SMAD1/5 and phospho-SMAD3 expression in neonatal cardiomyocytes in response to stimulation with 10 ng/mL BMP6 for the indicated times (data are representative of 3 experiments). Cross-sectional area (CSA; C) and [^{14}C] phenylalanine incorporation (E) of adult cardiomyocytes stimulated for 24 hours with FGF9, BMP6, or 10% FCS (75 to 111 cells per condition in C; 4 to 5 experiments in E; $^{**}P<0.01$, $^{***}P<0.001$ vs control). D, Images of adult cardiomyocytes stimulated for 24 hours with 300 ng/mL FGF9, 10 ng/mL BMP6, or 10% FCS. F, Immunoblot analysis of BMP6, phospho-SMAD1/5, and phospho-SMAD3 expression in the LVs of WT, tTA single transgenic, and tTA/FGF9 DTG mice 8 weeks after doxycycline withdrawal (similar results were obtained in 2 additional mice per genotype).

The effects of FGF9-stimulated HCAEC supernatants on neonatal cardiomyocyte size were reduced by 79% by a neutralizing anti-BMP6 antibody, indicating that BMP6 is responsible for a substantial part of the paracrine prohypertrophic effect (Figure 5A). Corroborating this finding, we found that recombinant BMP6 promoted a robust increase in cardiomyocyte size in concentrations as low as 1 ng/mL (Figure 5A). The effects of BMP6 on cardiomyocyte size were abolished by the ALK2/3/6 inhibitor dorsomorphin but not by the ALK4/5/7 inhibitor SB-431542 (Figure 5A). Similarly, BMP6 promoted an increase in cardiomyocyte protein content in an ALK2/3/6-dependent manner (Figure IV in the online-only Data Supplement). Consistent with signaling events downstream of ALK2/3/6,[23] BMP6 enhanced phosphorylation of SMAD1/5, but not SMAD3, in neonatal cardiomyocytes (Figure 5B).

Consistent with our observations in HCAECs, FGF9 stimulated proliferation and network formation of mouse heart endothelial cells (Figure VA and VB in the online-only Data Supplement), and FGF9-stimulated mouse endothelial cell supernatants promoted increases in neonatal cardiomyocyte size and protein content via paracrine release of BMP6 (Figure VC and VD in the online-only Data Supplement).

Like neonatal cardiomyocytes, adult cardiomyocytes responded to BMP6, but not FGF9, with a significant hypertrophic response characterized by increases in cross-sectional area (Figure 5C and 5D) and [^{14}C] phenylalanine incorporation (Figure 5E).

Eight weeks after doxycycline withdrawal, expression levels of BMP6 and phosphorylated SMAD1/5, but not phosphorylated SMAD3, were increased in the LVs of FGF9-expressing DTG mice, showing that FGF9 enhances the expression of BMP6 and activation of BMP6 downstream targets in vivo (Figure 5F).

LV Hypertrophy With Microvessel Expansion and Reduced Fibrosis After MI in FGF9-Expressing Mice

To explore the effects of transgenic FGF9 in the setting of MI, WT, tTA, and DTG mice underwent LAD ligation 2 weeks after doxycycline withdrawal and were followed up for an additional 6 weeks. Expression levels of endogenous FGF9 in the noninfarcted LV myocardium of WT mice did not change during this time period (Figure 6A). The ratio of scar length to endocardial circumference and scar thickness

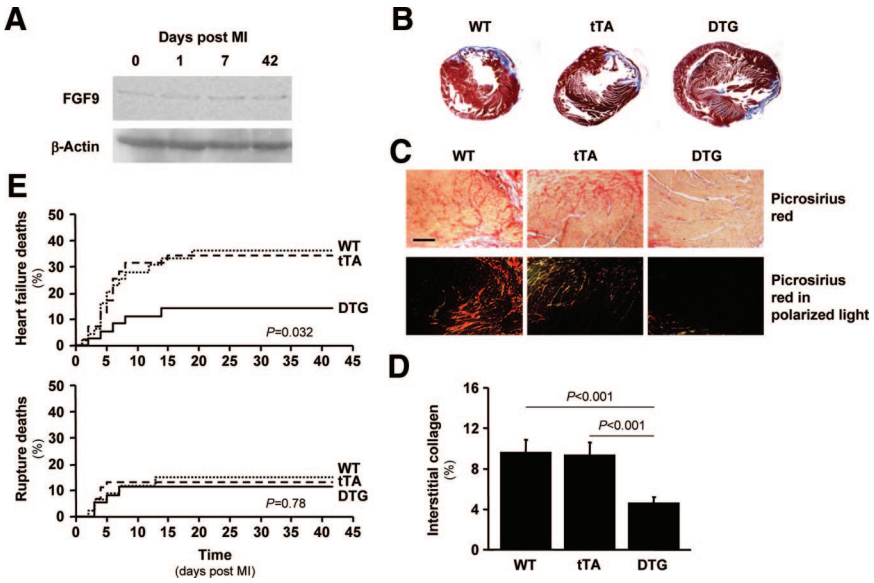

Figure 6. FGF9 reduces interstitial fibrosis and reduces heart failure mortality after MI. A, Immunoblot analysis of endogenous FGF9 expression in the noninfarcted LV myocardium of WT mice at various time points after LAD ligation (similar results were obtained in 2 additional mice per time point). B through E, Mice underwent LAD ligation 2 weeks after doxycycline withdrawal; end points were assessed 6 weeks later. B, Transverse sections of infarcted WT, tTA single transgenic, and tTA/FGF9 DTG hearts stained with Masson trichrome. C, Tissue sections from WT, tTA, and DTG hearts stained with Picrosirius Red and viewed under nonpolarized (top row) or polarized light (bottom row); images are from the noninfarcted part of the LV (scale bar, 200 μm). D, Quantification of interstitial collagen volume fraction in the noninfarcted LV myocardium (4 to 6 animals per group). E, Thirty-nine WT, 41 tTA, and 35 DTG mice were followed up for 6 weeks after LAD ligation.

were not significantly different between WT, tTA, and DTG mice (Figure 6B and Table 2). DTG animals, however, developed more LV hypertrophy with greater LV mass and ratio of LV mass to body mass compared with WT and tTA mice (Figure 6B and Table 2). Body weight was not significantly different between the genotypes (not shown). Enhanced LV hypertrophy in DTG mice was not related to differences in tail-cuff blood pressure or heart rate after MI (Figure I in the online-only Data Supplement, LAD ligation).

Postinfarct LV hypertrophy in DTG mice was characterized by a greater mean cardiomyocyte cross-sectional area, a higher density of $Ki67^+$ isolectin $B4^+$ endothelial cells, a greater capillary density, and an increased density of small (20 to 50 μm in diameter) αSMA^+ conductance vessels (Table 2). DTG mice developed less interstitial fibrosis in the noninfarcted LV myocardium compared with WT and tTA mice (Figure 6C and 6D). Induction of atrial natriuretic peptide and downregulation of αMHC and SERCA2a mRNA expression in the noninfarcted LV myocardium were attenuated in DTG mice (Table II in the online-only Data Supplement, LAD ligation).

Table 2. LV Histology 6 Weeks After LAD Ligation

	WT	tTA	DTG
Scar length/endocardial circumference, %	36±1	36±1	36±4
Scar thickness, mm	0.34±0.02	0.35±0.02	0.39±0.02
LV mass, mg	119±3	123±3	168±10†‖
LV mass/body mass, mg/g	4.2±0.2	4.4±0.2	5.5±0.4*§
Cardiomyocyte CSA, μm	754±40	746±34	892±36†‖
$Ki67^+$ isolectin $B4^+$ cell density (per field)	2.3±0.3	2.4±0.3	3.6±0.4*§
Capillary density (per CM)	1.3±0.1	1.3±0.1	1.7±0.1‡¶
αSMA^+ vessel density (per 100 CMs) (20-50 μm in diameter)	4.2±0.4	3.8±0.4	5.4±0.4*§
αSMA^+ vessel density (per 100 CMs) (>50 μm in diameter)	0.26±0.06	0.27±0.10	0.37±0.03

CSA indicates cross-sectional area; CM, cardiomyocyte. WT, tTA single transgenic, and tTA/FGF9 DTG mice were treated with doxycycline from mating until 8 weeks after birth. Doxycycline was then withdrawn. Mice underwent LAD ligation 2 weeks later and were followed up for an additional 6 weeks.

*$P<0.05$, †$P<0.01$, ‡$P<0.001$ versus WT; §$P<0.05$, ‖$P<0.01$, ¶$P<0.001$ versus tTA; 5 to 9 animals per group.

Improved Systolic Function and Reduced Heart Failure Mortality After MI in FGF9-Expressing Mice

As shown by invasive pressure-volume measurements, all 3 genotypes developed LV dilatation (increased LV end-diastolic volume, trend only in DTG mice) and systolic and diastolic dysfunction 6 weeks after MI (Table 1, LAD ligation). Systolic function, however, was more preserved in DTG compared with WT and tTA mice, as reflected by a smaller end-systolic volume and greater ejection fraction, cardiac output, stroke work, and dP/dtmax (Table 1, LAD ligation). Indexes of diastolic dysfunction (dP/dtmin, τ w) were not significantly different between DTG and control mice after MI (Table 1, LAD ligation). Typical pressure-volume loops are shown in Figure II in the online-only Data Supplement. Better systolic function in DTG mice after MI was confirmed by 2-dimensional echocardiography (Table III in the online-only Data Supplement, LAD ligation).

Six weeks after MI, 14 of 39 WT mice (36%), 14 of 41 tTA mice (34%), and 5 of 35 DTG mice (14%) had died with signs of heart failure ($P=0.032$; Figure 6E). Heart failure deaths occurred between days 1 and 19 after LAD ligation. Rupture deaths were observed less frequently in our FVB/N mice and were not significantly affected by transgenic FGF9 (WT, 6 of 39, 15%; tTA, 5 of 41, 12%; DTG, 4 of 35, 11%; $P=0.78$, Figure 6E). To explore how transgenic FGF9 reduces early heart failure mortality, echocardiography and LV histology were also performed 1 week after MI. Already at this early time point, significant increases in LV capillary density, cardiomyocyte cross-sectional area, wall thickness, and frac-

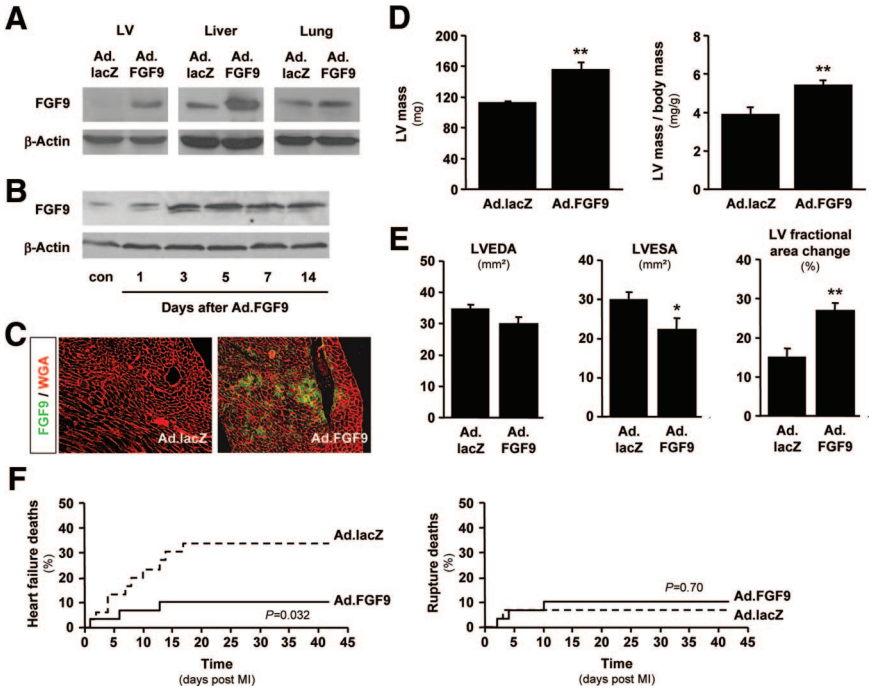

Figure 7. Adenoviral FGF9 gene transfer improves systolic function and reduces heart failure mortality after MI. WT mice underwent LAD ligation followed immediately by a single injection of Ad.lacZ or Ad.FGF9 into the LV cavity (1×10^8 pfu each). A, Immunoblot analysis of FGF9 expression in the noninfarcted LV myocardium, liver, and lung 7 days after gene transfer. B, Time course of FGF9 protein expression in the noninfarcted LV after FGF9 gene transfer. C, LV tissue sections stained with WGA and an anti-FGF9 antibody 7 days after Ad.lacZ or Ad.FGF9 treatment (images are from the noninfarcted LV). D, LV mass and ratio of LV mass to body mass 6 weeks after LAD ligation in 12 Ad.lacZ- and 14 Ad.FGF9-treated mice. E, LV end-diastolic area (LVEDA), LV end-systolic area (LVESA), and LV fractional area change 6 weeks after LAD ligation in 10 Ad.lacZ- and 10 Ad.FGF9-treated mice (*$P<0.05$, **$P<0.01$ vs Ad.lacZ). F, Thirty Ad.lacZ- and 30 Ad.FGF9-treated mice were followed up for 6 weeks after LAD ligation.

tional area change were observed in DTG mice, strongly suggesting that LV hypertrophy with enhanced systolic function contributed to the reduction in heart failure mortality (Table V in the online-only Data Supplement).

FGF9 Gene Transfer Improves Systolic Function and Reduces Heart Failure Mortality After MI

To further explore the therapeutic potential of FGF9 after MI, WT mice were treated with a single injection of Ad.FGF9 or Ad.lacZ into the LV cavity immediately after LAD ligation (1×10^8 plaque-forming units [pfu] per mouse). Seven days after adenoviral FGF9 gene transfer, FGF9 protein levels were increased in the noninfarcted LV and liver (Figure 7A). Increased FGF9 levels were detected in the noninfarcted LV as early as 3 days after gene transfer (Figure 7B). As shown by immunostaining 7 days after FGF9 gene transfer, FGF9 was expressed mostly in cardiomyocytes, with ≈30% to 35% of myocytes showing strong FGF9 expression (3 animals); an example is shown in Figure 7C.

Six weeks after LAD ligation, Ad.FGF9-treated mice displayed greater LV mass and ratio of LV mass to body mass (Figure 7D) and better systolic function with a smaller LV end-systolic area and greater LV fractional area change (Figure 7E) compared with Ad.lacZ-treated mice. Infarct sizes were not significantly different between the 2 groups (Ad.lacZ, 38±3%, n=6; Ad.FGF9, 37±4%, n=8).

Six weeks after MI, 10 of 30 Ad.lacZ-treated mice (33%) and 3 of 30 Ad.FGF9-treated mice (10%) had died with signs of heart failure ($P=0.032$; Figure 7F). Heart failure deaths occurred between days 1 and 18 after LAD ligation. Rupture deaths were observed less frequently and were not significantly affected by FGF9 (Ad.lacZ, 2 of 30, 7%; Ad.FGF9, 3 of 30, 10%; $P=0.70$; Figure 7F). Already 1 week after MI, significant increases in LV capillary density, cardiomyocyte cross-sectional area, wall thickness, and fractional area change were observed in Ad.FGF9-treated animals, suggesting again that FGF9-induced LV hypertrophy with enhanced systolic function contributed to the reduction in early heart failure mortality (Table VI in the online-only Data Supplement).

Discussion

In contrast to previous investigations in transgenic mice examining the function of FGF family members in the myocardium,[24–27] the inducible strategy used here bypassed any developmental effects that might have occurred in embryos or neonates and enabled us to explore the effects of FGF9 specifically in the adult heart. In unstressed mice, FGF9 stimulated concentric LV hypertrophy with microvessel expansion without increases in interstitial fibrosis and with no changes in the expression levels of cardiac genes that are typically observed during pathological hypertrophy and heart failure. Systolic and diastolic function was preserved in FGF9-expressing mice. FGF9-induced cardiac hypertrophy therefore displayed structural, molecular, and functional characteristics of the adaptive hypertrophic response that is observed after physiological increases in cardiac workload.[28–34]

In the setting of MI, transgenic FGF9 similarly promoted microvessel expansion and enhanced cardiomyocyte hypertrophy in the noninfarcted LV myocardium. Infarct sizes and scar thickness were not affected by myocardial expression of FGF9. Enhanced interstitial fibrosis, increased expression levels of atrial natriuretic peptide, a shift in MHC isoform expression from α to β, and decreased expression levels of SERCA2a are hallmarks of pathological hypertrophy, which develops in disease states with increased cardiac workload (eg, MI, valvular heart disease, hypertension) and may

ultimately lead to the development of heart failure.[33,34] FGF9 antagonized these structural and molecular features of pathological hypertrophy. Notably, FGF9 enhanced systolic function and reduced heart failure mortality after MI, thus clearly establishing that expression of FGF9 in the adult mouse myocardium is beneficial during recovery from an acute MI. Although interstitial LV fibrosis was attenuated and LV expression of SERCA2a was slightly augmented in FGF9-transgenic mice after MI, these parameters were still markedly abnormal compared with sham-operated mice, and diastolic function was not significantly enhanced by transgenic FGF9 (trend only for improvement in dP/dtmin).

Previous studies in animal models of pathological hypertrophy have shown that exercise training can promote extra LV hypertrophy with favorable changes in gene expression signatures and, as investigated in some reports, with improved systolic function.[35–37] Therefore, it has been proposed that stimulation of physiological hypertrophy, either by moderate exercise or by activation of signaling pathways promoting physiological hypertrophy, may be applied therapeutically in disease states, leading to pathological hypertrophy and heart failure.[29,38] Our study supports this emerging concept and provides the first evidence that a genetic intervention promoting a physiological-like increase in cardiac mass can lead to a marked reduction in heart failure mortality after MI. Consistent with previous reports,[20,21] fatal infarct ruptures were observed less frequently in our FVB/N mice and were not significantly influenced by myocardial expression of FGF9 in our study.

On a histological level, microvessel expansion and cardiomyocyte hypertrophy represented the main phenotypes of FGF9 transgenic mice, and our data indicate that they may be interrelated. Coordinated growth of the coronary microvasculature is important to ensure adequate tissue perfusion and to maintain contractile function as the myocyte compartment expands during cardiac development[3,4,39] or exercise-induced physiological hypertrophy.[30–32] Conversely, vascular rarefaction contributes to the decline in contractile function during chronic pressure overload–induced pathological hypertrophy.[40,41] An increase in $Ki67^+$ endothelial cells was the first phenotype observed after FGF9 induction in the myocardium, consistent with an initial stimulatory effect of cardiomyocyte-derived transgenic FGF9 on endothelial cell proliferation. In accord with this hypothesis, FGF9 stimulated angiogenesis in several bona fide angiogenesis assays in vitro (shown for both HCAECs and mouse cardiac endothelial cells) but did not promote considerable cardiomyocyte hypertrophy, as shown in neonatal and adult rat cardiomyocytes.

In the hypertrophied heart, proangiogenic cytokines are released from cardiomyocytes and signal to adjacent capillaries to stimulate myocardial angiogenesis.[40,41] Conversely, enhanced myocardial angiogenesis per se can induce cardiomyocyte hypertrophy in the absence of external stimuli, thus suggesting the existence of reciprocal, endothelial cell–derived prohypertrophic signals.[42,43] Conditioned supernatants from FGF9-stimulated endothelial cells (HCAECs or mouse cardiac endothelial cells) stimulated cardiomyocyte hypertrophy, which was mediated in part by paracrine release of the transforming growth factor-β cytokine family member BMP6. We found BMP6 to signal via BMP type I receptors ALK2/3/6, to activate SMAD 1/5, and to induce hypertrophy in neonatal and adult cardiomyocytes. BMP6 expression and SMAD1/5 phosphorylation were increased in the myocardium of FGF9 transgenic mice, confirming that FGF9 stimulates BMP6 signaling also in vivo. Of the many potential secondary paracrine effects induced by transgenic FGF9 in the myocardium, BMP6 therefore represents one potential mechanism whereby FGF9 promotes cardiomyocyte hypertrophy. We acknowledge the general limitations of using cell culture systems to provide mechanistic insight into in vivo phenotypes.

We have previously shown that intracoronary infusion of autologous BMCs enhances the recovery of systolic function in postinfarct patients,[13,44] and we have identified FGF9 as a factor that is secreted from these cells.[14] Given the results of the present study, FGF9-mediated paracrine effects in the border zone of the infarct may contribute to the improvements in microvascular perfusion and regional contractility that have been observed after intracoronary BMC transfer in some clinical trials.[13,16,45,46] Because FGF9 is 1 of >100 factors secreted from BMCs,[14] we do not infer that FGF9 "explains" the effects of cell therapy. Moreover, it has to be considered that our conditional transgenic and adenoviral approaches target the remote myocardium and border zone, whereas intracoronary cell transfer targets the border zone and infarcted area. Different therapeutic effects may therefore be observed in both situations (eg, hypertrophy of the remote myocardium has not been reported after BMC transfer). In any case, our data support the idea that secretome analyses of BMCs can lead to the identification of secreted factors with therapeutic activity after MI.[15,16]

Conclusions

Conditional expression of FGF9 in the adult mouse myocardium enhances vascularization and hypertrophy, which, when superimposed on postinfarct remodeling, promotes functional benefits and reduces heart failure mortality. The beneficial effects of transgenic FGF9 can be reproduced by adenoviral FGF9 gene transfer, which should stimulate further research into the therapeutic potential of FGF9 after MI.

Acknowledgment

We gratefully acknowledge Doris Gehring for helping us with the pressure-volume loop measurements.

Sources of Funding

This work was supported by the Deutsche Forschungsgemeinschaft, Klinische Forschergruppe 136 (Dr Wollert) and the Fondation Leducq (Drs Drexler, Sugden, and Molkentin).

Disclosures

None.

References

1. Velagaleti RS, Pencina MJ, Murabito JM, Wang TJ, Parikh NI, D'Agostino RB, Levy D, Kannel WB, Vasan RS. Long-term trends in the

incidence of heart failure after myocardial infarction. *Circulation*. 2008; 118:2057–2062.
2. Sutton MG, Sharpe N. Left ventricular remodeling after myocardial infarction: pathophysiology and therapy. *Circulation*. 2000;101: 2981–2988.
3. Bhattacharya S, Macdonald ST, Farthing CR. Molecular mechanisms controlling the coupled development of myocardium and coronary vasculature. *Clin Sci (Lond)*. 2006;111:35–46.
4. Lavine KJ, Ornitz DM. Shared circuitry: developmental signaling cascades regulate both embryonic and adult coronary vasculature. *Circ Res*. 2009;104:159–169.
5. Tanaka N, Mao L, DeLano FA, Sentianin EM, Chien KR, Schmid-Schonbein GW, Ross J Jr. Left ventricular volumes and function in the embryonic mouse heart. *Am J Physiol*. 1997;273:H1368–H1376.
6. Lavine KJ, Yu K, White AC, Zhang X, Smith C, Partanen J, Ornitz DM. Endocardial and epicardial derived FGF signals regulate myocardial proliferation and differentiation in vivo. *Dev Cell*. 2005;8:85–95.
7. Lavine KJ, White AC, Park C, Smith CS, Choi K, Long F, Hui CC, Ornitz DM. Fibroblast growth factor signals regulate a wave of Hedgehog activation that is essential for coronary vascular development. *Genes Dev*. 2006;20:1651–1666.
8. Itoh N, Ornitz DM. Functional evolutionary history of the mouse Fgf gene family. *Dev Dyn*. 2008;237:18–27.
9. Ornitz DM, Itoh N. Fibroblast growth factors. *Genome Biol*. 2001;2:1–12.
10. Spicer D. FGF9 on the move. *Nat Genet*. 2009;41:272–273.
11. Miyamoto M, Naruo K, Seko C, Matsumoto S, Kondo T, Kurokawa T. Molecular cloning of a novel cytokine cDNA encoding the ninth member of the fibroblast growth factor family, which has a unique secretion property. *Mol Cell Biol*. 1993;13:4251–4259.
12. Cardiogenomics. Available at: http://cardiogenomics.med.harvard.edu/home. Accessed February 27, 2010.
13. Wollert KC, Meyer GP, Lotz J, Ringes-Lichtenberg S, Lippolt P, Breidenbach C, Fichtner S, Korte T, Hornig B, Messinger D, Arseniev L, Hertenstein B, Ganser A, Drexler H. Intracoronary autologous bone-marrow cell transfer after myocardial infarction: the BOOST randomised controlled clinical trial. *Lancet*. 2004;364:141–148.
14. Korf-Klingebiel M, Kempf T, Sauer T, Brinkmann E, Fischer P, Meyer GP, Ganser A, Drexler H, Wollert KC. Bone marrow cells are a rich source of growth factors and cytokines: implications for cell therapy trials after myocardial infarction. *Eur Heart J*. 2008;29:2851–2858.
15. Gnecchi M, Zhang Z, Ni A, Dzau VJ. Paracrine mechanisms in adult stem cell signaling and therapy. *Circ Res*. 2008;103:1204–1219.
16. Wollert KC, Drexler H. Cell therapy for the treatment of coronary heart disease: a critical appraisal. *Nat Rev Cardiol*. 2010;7:204–215.
17. Yu PB, Hong CC, Sachidanandan C, Babitt JL, Deng DY, Hoyng SA, Lin HY, Bloch KD, Peterson RT. Dorsomorphin inhibits BMP signals required for embryogenesis and iron metabolism. *Nat Chem Biol*. 2008; 4:33–41.
18. Inman GJ, Nicolas FJ, Callahan JF, Harling JD, Gaster LM, Reith AD, Laping NJ, Hill CS. SB-431542 is a potent and specific inhibitor of transforming growth factor-beta superfamily type I activin receptor-like kinase (ALK) receptors ALK4, ALK5, and ALK7. *Mol Pharmacol*. 2002;62:65–74.
19. Sanbe A, Gulick J, Hanks MC, Liang Q, Osinska H, Robbins J. Reengineering inducible cardiac-specific transgenesis with an attenuated myosin heavy chain promoter. *Circ Res*. 2003;92:609–616.
20. Gao XM, Xu Q, Kiriazis H, Dart AM, Du XJ. Mouse model of post-infarct ventricular rupture: time course, strain- and gender-dependency, tensile strength, and histopathology. *Cardiovasc Res*. 2005;65:469–477.
21. van den Borne SW, van de Schans VA, Strzelecka AE, Vervoort-Peters HT, Lijnen PM, Cleutjens JP, Smits JF, Daemen MJ, Janssen BJ, Blankesteijn WM. Mouse strain determines the outcome of wound healing after myocardial infarction. *Cardiovasc Res*. 2009;84: 273–282.
22. Lim YC, Luscinskas FW. Isolation and culture of murine heart and lung endothelial cells for in vitro model systems. *Methods Mol Biol*. 2006; 341:141–154.
23. Derynck R, Zhang YE. Smad-dependent and Smad-independent pathways in TGF-β family signalling. *Nature*. 2003;425:577–584.
24. Fernandez B, Buehler A, Wolfram S, Kostin S, Espanion G, Franz WM, Niemann H, Doevendans PA, Schaper W, Zimmermann R. Transgenic myocardial overexpression of fibroblast growth factor-1 increases coronary artery density and branching. *Circ Res*. 2000;87:207–213.
25. House SL, Bolte C, Zhou M, Doetschman T, Klevitsky R, Newman G, Schultz Jel J. Cardiac-specific overexpression of fibroblast growth factor-2 protects against myocardial dysfunction and infarction in a murine model of low-flow ischemia. *Circulation*. 2003;108:3140–3148.
26. Palmen M, Daemen MJ, De Windt LJ, Willems J, Dassen WR, Heeneman S, Zimmermann R, Van Bilsen M, Doevendans PA. Fibroblast growth factor-1 improves cardiac functional recovery and enhances cell survival after ischemia and reperfusion: a fibroblast growth factor receptor, protein kinase C, and tyrosine kinase-dependent mechanism. *J Am Coll Cardiol*. 2004;44:1113–1123.
27. Liao S, Bodmer J, Pietras D, Azhar M, Doetschman T, Schultz Jel J. Biological functions of the low and high molecular weight protein isoforms of fibroblast growth factor-2 in cardiovascular development and disease. *Dev Dyn*. 2009;238:249–264.
28. Dorn GW II, Robbins J, Sugden PH. Phenotyping hypertrophy: eschew obfuscation. *Circ Res*. 2003;92:1171–1175.
29. Dorn GW II. The fuzzy logic of physiological cardiac hypertrophy. *Hypertension*. 2007;49:962–970.
30. Tomanek RJ. Response of the coronary vasculature to myocardial hypertrophy. *J Am Coll Cardiol*. 1990;15:528–533.
31. Shiojima I, Sato K, Izumiya Y, Schiekofer S, Ito M, Liao R, Colucci WS, Walsh K. Disruption of coordinated cardiac hypertrophy and angiogenesis contributes to the transition to heart failure. *J Clin Invest*. 2005; 115:2108–2118.
32. Walsh K, Shiojima I. Cardiac growth and angiogenesis coordinated by intertissue interactions. *J Clin Invest*. 2007;117:3176–3179.
33. Samuel JL, Corda S, Chassagne C, Rappaport L. The extracellular matrix and the cytoskeleton in heart hypertrophy and failure. *Heart Fail Rev*. 2000;5:239–250.
34. Lompre AM, Hajjar RJ, Harding SE, Kranias EG, Lohse MJ, Marks AR. Ca^{2+} cycling and new therapeutic approaches for heart failure. *Circulation*. 2010;121:822–830.
35. Scheuer J, Malhotra A, Hirsch C, Capasso J, Schaible TF. Physiologic cardiac hypertrophy corrects contractile protein abnormalities associated with pathologic hypertrophy in rats. *J Clin Invest*. 1982;70:1300–1305.
36. Freimann S, Scheinowitz M, Yekutieli D, Feinberg MS, Eldar M, Kessler-Icekson G. Prior exercise training improves the outcome of acute myocardial infarction in the rat. Heart structure, function, and gene expression. *J Am Coll Cardiol*. 2005;45:931–938.
37. Konhilas JP, Watson PA, Maass A, Boucek DM, Horn T, Stauffer BL, Luckey SW, Rosenberg P, Leinwand LA. Exercise can prevent and reverse the severity of hypertrophic cardiomyopathy. *Circ Res*. 2006;98: 540–548.
38. McMullen JR, Amirahmadi F, Woodcock EA, Schinke-Braun M, Bouwman RD, Hewitt KA, Mollica JP, Zhang L, Zhang Y, Shioi T, Buerger A, Izumo S, Jay PY, Jennings GL. Protective effects of exercise and phosphoinositide 3-kinase(p110α) signaling in dilated and hypertrophic cardiomyopathy. *Proc Natl Acad Sci U S A*. 2007;104:612–617.
39. Giordano FJ, Gerber HP, Williams SP, VanBruggen N, Bunting S, Ruiz-Lozano P, Gu Y, Nath AK, Huang Y, Hickey R, Dalton N, Peterson KL, Ross J Jr, Chien KR, Ferrara N. A cardiac myocyte vascular endothelial growth factor paracrine pathway is required to maintain cardiac function. *Proc Natl Acad Sci U S A*. 2001;98:5780–5785.
40. Heineke J, Auger-Messier M, Xu J, Oka T, Sargent MA, York A, Klevitsky R, Vaikunth S, Duncan SA, Aronow BJ, Robbins J, Cromblehol TM, Molkentin JD. Cardiomyocyte GATA4 functions as a stress-responsive regulator of angiogenesis in the murine heart. *J Clin Invest*. 2007;117:3198–3210.
41. Sano M, Minamino T, Toko H, Miyauchi H, Orimo M, Qin Y, Akazawa H, Tateno K, Kayama Y, Harada M, Shimizu I, Asahara T, Hamada H, Tomita S, Molkentin JD, Zou Y, Komuro I. p53-induced inhibition of Hif-1 causes cardiac dysfunction during pressure overload. *Nature*. 2007; 446:444–448.
42. Tirziu D, Chorianopoulos E, Moodie KL, Palac RT, Zhuang ZW, Tjwa M, Roncal C, Eriksson U, Fu Q, Elfenbein A, Hall AE, Carmeliet P, Moons L, Simons M. Myocardial hypertrophy in the absence of external stimuli is induced by angiogenesis in mice. *J Clin Invest*. 2007;117: 3188–3197.
43. Hsieh PC, Davis ME, Lisowski LK, Lee RT. Endothelial-cardiomyocyte interactions in cardiac development and repair. *Annu Rev Physiol*. 2006; 68:51–66.
44. Meyer GP, Wollert KC, Lotz J, Steffens J, Lippolt P, Fichtner S, Hecker H, Schaefer A, Arseniev L, Hertenstein B, Ganser A, Drexler H. Intracoronary bone marrow cell transfer after myocardial infarction: eighteen months' follow-up data from the randomized, controlled BOOST (Bone

Marrow Transfer to Enhance ST-Elevation Infarct Regeneration) trial. *Circulation*. 2006;113:1287–1294.
45. Schachinger V, Erbs S, Elsasser A, Haberbosch W, Hambrecht R, Holschermann H, Yu J, Corti R, Mathey DG, Hamm CW, Suselbeck T, Assmus B, Tonn T, Dimmeler S, Zeiher AM. Intracoronary bone marrow-derived progenitor cells in acute myocardial infarction. *N Engl J Med*. 2006;355:1210–1221.
46. Erbs S, Linke A, Schachinger V, Assmus B, Thiele H, Diederich KW, Hoffmann C, Dimmeler S, Tonn T, Hambrecht R, Zeiher AM, Schuler G. Restoration of microvascular function in the infarct-related artery by intracoronary transplantation of bone marrow progenitor cells in patients with acute myocardial infarction: the Doppler Substudy of the Reinfusion of Enriched Progenitor Cells and Infarct Remodeling in Acute Myocardial Infarction (REPAIR-AMI) trial. *Circulation*. 2007;116:366–374.

CLINICAL PERSPECTIVE

Paracrine mechanisms are thought to contribute to the beneficial effects of bone marrow cells on perfusion and function of the infarcted heart that have been demonstrated in experimental studies and some clinical trials. We have previously identified fibroblast growth factor 9 (FGF9) as 1 of >100 paracrine factors that are secreted from bone marrow cells after myocardial infarction. In the embryonic heart, FGF9 is expressed by the epicardium and endocardium and provides an epithelial-to-mesenchymal signal to stimulate coronary artery formation and cardiomyoblast expansion in the developing myocardium. FGF9, however, is expressed only at very low levels in the adult heart. Using a tetracycline-responsive binary transgene system based on the α-myosin heavy chain promoter, we show here that conditional expression of FGF9 in the adult mouse myocardium supports functional adaptation and survival after myocardial infarction. Transgenic FGF9 stimulated left ventricular hypertrophy with microvessel expansion, reduced interstitial fibrosis, attenuated fetal gene expression, preserved diastolic but improved systolic function, and markedly reduced heart failure mortality. A single injection of an adenoviral vector encoding FGF9 promoted similar improvements in left ventricular systolic function and survival after myocardial infarction. Mechanistically, FGF9 acted primarily on endothelial cells to promote angiogenesis and paracrine release of prohypertrophic factors, including bone morphogenetic protein 6. These observations support the idea that secretome analyses in bone marrow cells can lead to the identification of secreted factors with therapeutic activity after myocardial infarction. Specifically, the data suggest a previously unrecognized therapeutic potential for FGF9 after myocardial infarction.

SUPPLEMENTAL MATERIAL

EXPANDED METHODS

Materials

Recombinant mouse and human fibroblast growth factor (FGF) 9, mouse bone morphogenetic protein (BMP) 6, a neutralizing anti-BMP6 antibody and a corresponding isotype control antibody were purchased from R&D Systems (Minneapolis, MN). Mouse and rat cells were stimulated with mouse FGF9 and BMP6, human cells with human FGF9. Endothelin 1 (ET1), dorsomorphin, an inhibitor of activin receptor-like kinase (ALK) 2, ALK3, and ALK6,[1] and SB-431542, an inhibitor of ALK4, ALK5, and ALK7,[2] were purchased from Sigma-Aldrich (St. Louis, MO).

Inducible cardiac-specific FGF9-transgenic mice and animal procedures

A tetracycline-responsive transgene system[3] was used to allow temporally-regulated expression of FGF9 in adult cardiac myocytes. Mouse FGF9 cDNA was cloned into the *Sal*I–*Hind*III site of the chimeric tetracycline-responsive α myosin heavy chain (MHC) promoter (responder mice). The construct was linearized and injected into FVB/N pronuclei. Founder lines were crossed with transgenic mice expressing the tetracycline transactivator (tTA) under the control of the constitutive αMHC promoter (FVB/N background). Doxycycline (Dox) was provided in the drinking water (625 mg/L) from mating up to 8 weeks after birth to inhibit transgenic FGF9 expression; Dox was withdrawn thereafter, resulting in expression of FGF9. Transgenes were detected in genomic DNA by PCR using the primers
5'-GTCGTAATAATGGCGGCATACTATC-3' and
5'-AGCGCATTAGAGCTGCTTAATGAGGTC-3' for the tTA driver transgene, and

5’-GCAGGACTGGATTTCATTTAGAG-3’ and 5’-CCTGAGATTAGGAGTTGGAGAC-3’ for the FGF9 responder transgene.

Myocardial infarction (MI) was induced in male mice by permanent left anterior descending coronary artery (LAD) ligation.[4] Animals were anesthetized with 3% isoflurane and ventilated with 1 to 2% isoflurane (Baxter, Deerfield, IL). Control male mice underwent a sham operation where the ligature around the LAD was not tied. No differences in perioperative mortality rates (first 24 h) were observed between wild type, tTA single transgenic, and FGF9/tTA double transgenic mice. For an assessment of postinfarct survival, mice were followed and inspected daily from 24 h up to 6 weeks after surgery. Autopsies were performed on all dead animals, rupture was diagnosed by the presence of a blood clot around the heart and in the chest cavity, whereas heart failure was diagnosed by chest fluid accumulation.[5,6] Six weeks after a sham operation, no deaths were observed in any of the genotypes. All animal procedures were approved by our local state authorities.

Adenoviral FGF9 gene transfer

Mouse FGF9 cDNA was cloned into a replication-deficient adenovirus using the AdEasy XL Vector System (Stratagene, La Jolla, CA). A replication-deficient adenovirus encoding β-galactosidase was used as control. Viruses were purified with the Adeno-X Virus Purification Kit (BD Biosciences, Franklin Lakes, NJ). Viruses were injected into the left ventricular (LV) cavity immediately after LAD ligation.

In vivo pressure-volume measurements

Left ventricular pressure-volume (P-V) loops were recorded with a 1.4 F micromanometer conductance catheter (SPR-839, Millar Instruments, Houston, TX) inserted via the right carotid

artery during isoflurane (2%) anesthesia. Steady-state P-V loops were sampled at a rate of 1 kHz and analyzed by a sample-blinded investigator (T.K.).

Echocardiography

Transthoracic echocardiography was performed with a linear 30 MHz transducer (VisualSonics, Toronto, Canada) in mice that were sedated with 1 to 1.5% isoflurane and placed on a heating pad to maintain body temperature. LV end-diastolic area (LVEDA) and end-systolic area (LVESA) were recorded from the long-axis parasternal view. Fractional area change was calculated as [(LVEDA–LVESA)/LVEDA] × 100.

Histology

Left ventricles were fixed in phosphate-buffered 4% formaldehyde and embedded in paraffin. Sections (5 μm in thickness) were cut from basal, midventricular, and apical LV slices and stained with Masson's trichrome which shows fibrosis in blue. To determine infarct size, scar length and total LV circumference were traced at the endocardial surface. Infarct sizes were calculated as the average ratio of scar length to total LV circumference in basal, midventricular, and apical sections. Scar thickness was measured at the center of the infarct in the same sections and averaged.

For fluorescent (immuno)staining, midventricular slices of the left ventricle were embedded in OCT compound and frozen at -80°C. Cryosections (5 μm in thickness) were stained with TRITC-conjugated wheat germ agglutinin (WGA, Sigma-Aldrich) to outline cardiomyocytes. The circumferences of 40 to 50 myocytes were traced and digitized to calculate mean cardiomyocyte cross-sectional area. Only cells from fields with circular myocyte shapes (indicative of a transverse section) were analyzed. Ki67 was detected with a rabbit polyclonal antibody and a Cy5-labeled secondary antibody from Abcam (Cambridge, MA). Fluorescein-labeled GSL I-isolectin B4

(Vector Laboratories, Burlingame, CA) was used to visualize capillaries. Conductance vessels were identified by their diameter (>20 μm) after immunostaining for smooth muscle α-actin (SMA) using a mouse monoclonal antibody from Sigma-Aldrich and a FITC-labeled secondary antibody from Abcam. Troponin T was visualized with a mouse monoclonal antibody from Abcam and an Alexa Fluor 594-labeled secondary antibody from Invitrogen (Carlsbad, CA). Interstitial collagen content was determined by picrosirius red polarization microscopy. Interstitial collagen volume fraction was calculated as the sum of all connective tissue areas divided by the sum of all connective tissue and muscle areas in the respective field. Perivascular areas were not included in the analysis. Images were acquired with an Axiovert microscope (Carl Zeiss, Jena, Germany).

Quantitative PCR (qPCR)

Total RNA was extracted from LV myocardium by TRIzol (Invitrogen) and purified with RNeasy kits (Qiagen, Hilden, Germany). After reverse transcription (Superscript II, Invitrogen), qPCR was performed using the Brilliant SYBR Green Mastermix-Kit and the MX4000 multiplex QPCR System from Stratagene (PCR primers are shown in Supplemental Table 1).

Cell culture

Human coronary artery endothelial cells (HCAECs) were purchased from Provitro (Berlin, Germany) and grown in MCDB131 medium (Invitrogen) supplemented with 10% FCS. Cells from passage 3 to 7 were used. Mouse heart endothelial cells were isolated from 10-day old C57/BL6 mice as previously described.[7] In brief, ventricles were digested in collagenase I solution (265 U per heart) followed by magnetic cell sorting using Dynabeads (Invitrogen) coated with a rat anti-mouse CD31 monoclonal antibody (BD Biosciences). Prior to their use in functional assays, endothelial cells were cultured overnight in MCDB131 (HCAECs) or D-MEM/high glucose

medium (mouse endothelial cells) containing 0.5% FCS. Endothelial cell proliferation was measured by bromodeoxyuridine incorporation in 96-well plates (5×10^3 cells per well). Network formation was assayed in 24-well plates (3×10^4 cells per well) coated with growth factor-reduced Matrigel (BD Biosciences).[8]

Ventricular cardiomyocytes were isolated from 1 to 3-day-old Sprague-Dawley rats by Percoll density gradient centrifugation.[8] Cell size was determined by planimetry, protein content by the Bradford assay. Adult ventricular cardiomyocytes were isolated from 4-month-old Wistar rats.[9] Cross-sectional area of adult cardiomyocytes was calculated as $(\text{cell width}/2)^2 \times \pi$.
Net protein synthesis was measured by [^{14}C] phenylalanine incorporation.

Immunoblotting

Antibodies against mouse FGF9 (Genway Biotech, San Diego, CA), BMP6 (Santa Cruz Biotechnology, Santa Cruz, CA), phospho-SMAD1/5, phospho-SMAD3, and β-actin (Cell Signaling Technology, Danvers, MA) were used for immunoblotting.

Antibody array

HCAECs (1×10^6 cells) were cultured in 2 mL MCDB131 without FCS for 24 h in the presence or absence of FGF9 (10 ng/mL). Human Cytokine ProteinChip Array C Series 2000 membranes (Ray Biotech, Norcross, GA) targeting 174 secreted factors were incubated with 1 mL of conditioned HCAEC supernatant for 2 h, washed, and sequentially incubated with biotinylated antibodies, horseradish peroxidase-conjugated strepavidin, and detection solution according to the manufacturer's instructions.

REFERENCES

1. Yu PB, Hong CC, Sachidanandan C, Babitt JL, Deng DY, Hoyng SA, Lin HY, Bloch KD, Peterson RT. Dorsomorphin inhibits BMP signals required for embryogenesis and iron metabolism. *Nat Chem Biol.* 2008;4:33-41.

2. Inman GJ, Nicolas FJ, Callahan JF, Harling JD, Gaster LM, Reith AD, Laping NJ, Hill CS. SB-431542 is a potent and specific inhibitor of transforming growth factor-beta superfamily type I activin receptor-like kinase (ALK) receptors ALK4, ALK5, and ALK7. *Mol Pharmacol.* 2002;62:65-74.

3. Sanbe A, Gulick J, Hanks MC, Liang Q, Osinska H, Robbins J. Reengineering inducible cardiac-specific transgenesis with an attenuated myosin heavy chain promoter. *Circ Res.* 2003;92:609-616.

4. Fuchs M, Hilfiker A, Kaminski K, Hilfiker-Kleiner D, Guener Z, Klein G, Podewski E, Schieffer B, Rose-John S, Drexler H. Role of interleukin-6 for LV remodeling and survival after experimental myocardial infarction. *Faseb J.* 2003;17:2118-2120.

5. Gao XM, Xu Q, Kiriazis H, Dart AM, Du XJ. Mouse model of post-infarct ventricular rupture: time course, strain- and gender-dependency, tensile strength, and histopathology. *Cardiovasc Res.* 2005;65:469-477.

6. van den Borne SW, van de Schans VA, Strzelecka AE, Vervoort-Peters HT, Lijnen PM, Cleutjens JP, Smits JF, Daemen MJ, Janssen BJ, Blankesteijn WM. Mouse strain determines the outcome of wound healing after myocardial infarction. *Cardiovasc Res.* 2009;84:273-282.

7. Lim YC, Luscinskas FW. Isolation and culture of murine heart and lung endothelial cells for in vitro model systems. *Methods Mol Biol.* 2006;341:141-154.

8. Korf-Klingebiel M, Kempf T, Sauer T, Brinkmann E, Fischer P, Meyer GP, Ganser A, Drexler H, Wollert KC. Bone marrow cells are a rich source of growth factors and cytokines: implications for cell therapy trials after myocardial infarction. *Eur Heart J.* 2008;29:2851-2858.

9. Schluter KD, Schreiber D. Adult ventricular cardiomyocytes: isolation and culture. *Methods Mol Biol.* 2005;290:305-314.

Supplemental Table 1. PCR primers

	Forward	**Reverse**
ANP	5'-GTGGCTTGTGGGAAAATA GTTGA-3'	5'-CTGGCTTGATGATCTGCCT TTAC-3'
αMHC	5'-CCAATGAGTACCGCGTGA A-3'	5'-ATGTGCCGGACCTTGGAA-3'
βMHC	5'-CTTGTTGACCTGGGACTCG G-3'	5'-ACCTGTCCAAGTTCCGCAA G-3'
SERCA2a	5'-TGTTCATTCTGGACAGAGT GGAAGG-3'	5'-TTAATAAAGTTGGCAGAGT CCTCAAGG-3'
Phospholamban	5'-TCAGAGAAGCATCACGAT GATACAGATCAG-3'	5'-ATGGAAAAAGTGCAATAC CTCACTCGC-3'
GAPDH	5'-GCAGGATGCATTGCTGAC AATC-3'	5'-CTGAGTATGTCGTGGAGTC TACTG-3'

ANP, atrial natriuretic peptide; MHC, myosin heavy chain; SERCA2a, sarco(endo)plasmic reticulum Ca^{2+} ATPase-2a; GAPDH, glyceraldehyde-3-phosphate dehydrogenase.

Supplemental Table 2. Gene expression levels 6 weeks after sham operation or LAD ligation

	WT	**tTA**	**DTG**
Sham			
ANP	100 ± 15	86 ± 16	90 ± 10
αMHC	100 ± 10	116 ± 8	97 ± 5
βMHC	100 ± 4	97 ± 11	90 ± 19
SERCA2a	100 ± 6	78 ± 10	86 ± 7
Phospholamban	100 ± 9	94 ± 2	104 ± 5
LAD ligation			
ANP	895 ± 105**	937 ± 94***	505 ± 197**,†,‡
αMHC	29 ± 15***	39 ± 16***	83 ± 21††,‡‡
βMHC	113 ± 7	116 ± 2	110 ± 5
SERCA2a	16 ± 2**	20 ± 4***	34 ± 4**,†,‡
Phospholamban	67 ± 9	67 ± 9	69 ± 11

WT, tTA single transgenic, and tTA/FGF9 double transgenic (DTG) mice were treated with Dox from mating until 8 weeks after birth. Dox was then withdrawn. Mice underwent a sham operation or LAD ligation 2 weeks after Dox withdrawal. LV gene expression levels were determined by qPCR 6 weeks later (non-infarcted LV myocardium in infarcted mice). Data were normalized to glyceraldehyde-3-phosphate dehydrogenase expression and expressed as (%) of sham-operated WT mice. ANP, atrial natriuretic peptide; MHC, myosin heavy chain; SERCA2a, sarco(endo)plasmic reticulum Ca^{2+} ATPase-2a. ***P*<0.01, ****P*<0.001 vs. same genotype sham; †*P*<0.05, ††*P*<0.01 vs. WT LAD ligation; ‡*P*<0.05, ‡‡*P*<0.01 vs. tTA LAD ligation; 5-6 animals per group.

Supplemental Table 3. Echocardiography 6 weeks after sham operation or LAD ligation

	WT	**tTA**	**DTG**
Sham			
Heart rate (min^{-1})	461 ± 12	453 ± 11	443 ± 25
LV posterior wall thickness (mm)	1.23 ± 0.05	1.22 ± 0.05	1.34 ± 0.03†,‡
LV end-diastolic area (mm^2)	26.4 ± 0.5	26.8 ± 0.6	27.4 ± 0.5
LV end-systolic area (mm^2)	15.6 ± 0.5	16.5 ± 0.6	16.3 ± 0.4
LV fractional area change (%)	41.3 ± 1.1	38.7 ± 1.3	41.2 ± 1.1
LAD ligation			
Heart rate (min^{-1})	444 ± 18	449 ± 13	418 ± 13
LV posterior wall thickness (mm)	1.44 ± 0.08**	1.38 ± 0.11*	1.69 ± 0.07***,†,‡‡
LV end-diastolic area (mm^2)	34.0 ± 1.3**	33.3 ± 2.0**	31.8 ± 1.0**
LV end-systolic area (mm^2)	28.0 ± 1.6***	27.8 ± 2.1***	22.2 ± 1.5***,†,‡
LV fractional area change (%)	18.3 ± 2.5***	17.9 ± 2.4***	29.1 ± 2.6***,†,‡

WT, tTA single transgenic, and tTA/FGF9 double transgenic (DTG) mice were treated with Dox from mating until 8 weeks after birth. Dox was then withdrawn. Mice underwent a sham operation or LAD ligation 2 weeks after Dox withdrawal. Echocardiography was performed 6 weeks later. LV, left ventricular. *P<0.05, **P<0.01, ***P<0.001 vs. same genotype sham; †P<0.05 vs. WT sham or WT LAD ligation; ‡P<0.05, ‡‡P<0.01 vs. tTA sham or tTA LAD ligation; 8-13 animals per group.

Supplemental Table 4. Secreted factors induced by FGF9 in HCAECs

	Average induction	Array #1			Array #2		
		Control	FGF9	x-fold	Control	FGF9	x-fold
BMP6	**4.7**	16757	41250	2.5	7055	47740	6.8
IGFBP4	**3.7**	30518	61296	2.0	10660	57043	5.4
CXCL13	**3.1**	6849	22901	3.3	20105	55765	2.8
BMP4	**2.8**	20032	46847	2.3	16979	55647	3.3
IL10	**2.3**	5646	11051	2.0	14607	38312	2.6
FGF6	**2.3**	13047	30197	2.3	16452	36964	2.2
IL6	**2.2**	30877	62891	2.0	192737	434177	2.3
CCL2	**2.2**	59196	133467	2.3	79456	160433	2.0
PDGFA	**2.1**	20369	42035	2.1	33555	70668	2.1

Human coronary artery endothelial cells (HCAECs) were kept under control conditions or stimulated with 10 ng/mL FGF9 for 24 h. Antibody arrays detecting 174 secreted factors were incubated with conditioned HCAEC supernatants. Data from two independent experiments are shown. Nine secreted factors were induced ≥2-fold by FGF9 in both experiments, and are listed here according to their average (mean) induction by FGF9 vs. control. BMP, bone morphogenetic protein; IGFBP4, insulin-like growth factor binding protein 4; CXCL13, chemokine (C-X-C motif) ligand 13; IL, interleukin; FGF6, fibroblast growth factor 6; CCL2, chemokine (C-C motif) ligand 2; PDGFA, platelet-derived growth factor α polypeptide.

Supplemental Table 5. Echocardiography and histology 1 week after LAD ligation

	WT	**tTA**	**DTG**
Heart rate (min^{-1})	498 ± 17	441 ± 13	473 ± 13
LV posterior wall thickness (mm)	1.18 ± 0.13	1.29 ± 0.06	1.55 ± 0.06*,†
LV end-diastolic area (mm^2)	27.7 ± 1.4	24.1 ± 0.6	23.5 ± 0.9
LV end-systolic area (mm^2)	21.7 ± 1.3	19.4 ± 1.1	14.6 ± 0.8**,†
LV fractional area change (%)	20.7 ± 1.4	20.3 ± 2.7	36.6 ± 2.1***,†
Cardiomyocyte CSA (μm^2)	582 ± 29	494 ± 27	806 ± 9*,†
Capillary density (per CM)	1.1 ± 0.0	1.1 ± 0.0	1.3 ± 0.1*,†

WT, tTA single transgenic, and tTA/FGF9 double transgenic (DTG) mice were treated with Dox from mating until 8 weeks after birth. Dox was then withdrawn. Mice underwent LAD ligation 2 weeks after Dox withdrawal. Echocardiography and histological analyses (non-infarcted left ventricle) were performed 1 week later. LV, left ventricular; CSA, cross sectional area; CM, cardiomyocyte. *P<0.05, **P<0.01, ***P<0.001 vs. WT; †P<0.05 vs. tTA; 5-7 animals per group.

Supplemental Table 6. Echocardiography and histology 1 week after LAD ligation

	Ad.lacZ	**Ad.FGF9**
Heart rate (min^{-1})	446 ± 12	445 ± 5
LV posterior wall thickness (mm)	1.29 ± 0.04	1.52 ± 0.06*
LVEDA (mm^2)	30.4 ± 1.4	26.7 ± 1.2
LVESA (mm^2)	27.8 ± 1.3	21.3 ± 1.5*
LV fractional area change (%)	10.3 ± 1.1	21.0 ± 2.8*
Cardiomyocyte CSA (μm^2)	608 ± 21	823 ± 28***
Capillary density (per CM)	1.2 ± 0.0	1.5 ± 0.1*

Wild-type mice underwent LAD ligation immediately followed by a single injection of Ad.lacZ or Ad.FGF9 into the left ventricular (LV) cavity (1×10^8 p.f.u., each). Echocardiography and histological analyses (non-infarcted left ventricle) were performed 1 week later. CSA, cross sectional area; CM, cardiomyocyte. *P<0.05, ***P<0.001 vs. Ad.lacZ; 4-9 animals per group.

SUPPLEMENTAL FIGURE LEGENDS

Supplemental Figure 1. *Tail-cuff blood pressure*

WT, tTA single transgenic, and tTA/FGF9 double transgenic (DTG) mice were treated with Dox from mating until 8 weeks after birth. Dox was then withdrawn. Mice underwent a sham operation or LAD ligation at the age of 10 weeks, and were followed for an additional 6 weeks. Serial tail-cuff (A) blood pressure and (B) heart rate measurements were obtained in awake mice. The number of animals is shown in each bar.

Supplemental Figure 2. *Left ventricular pressure-volume loops*

WT, tTA single transgenic, and tTA/FGF9 double transgenic (DTG) mice were treated with Dox from mating until 8 weeks after birth. Dox was then withdrawn. Mice underwent a sham operation or LAD ligation 2 weeks after Dox withdrawal. Invasive left ventricular (LV) pressure-volume (P-V) measurements were performed 6 weeks later. Typical steady-state P-V loops are shown.

Supplemental Figure 3. *FGF9 does not increase protein content in neonatal cardiomyocytes*

Protein content of neonatal cardiomyocytes stimulated for 24 h with 100 nmol/L endothelin 1 (ET1) or increasing concentrations of FGF9 (4 experiments; **P*<0.05 vs. control).

Supplemental Figure 4. *BMP6 increases protein content in neonatal cardiomyocytes in an ALK2/3/6-dependent manner*

Protein content of neonatal cardiomyocytes stimulated for 24 h with 100 nmol/L endothelin 1 (ET1) or increasing concentrations of BMP6. Where indicated, cells were treated with the ALK2/3/6 inhibitor dorsomorphin (DM, 20 μmol/L) or the ALK4/5/7 inhibitor SB-431542

(SB, 20 μmol/L) (4 experiments; **P*<0.05 vs. control).

Supplemental Figure 5. *FGF9 stimulates mouse endothelial cell proliferation, network formation, and release of pro-hypertrophic BMP6*

(A) Proliferation and (B) network formation of mouse heart endothelial cells (MHEC) stimulated for 24 h with 10 ng/mL vascular endothelial growth factor (VEGF) or increasing concentrations of FGF9 (4 experiments; **P*<0.05, ***P*<0.01 vs. control). (C and D) Neonatal cardiomyocytes were cultured for 24 h in the absence (control) or presence of endothelin 1 (ET1, 100 nmol/L). Additional cardiomyocytes were stimulated for 24 h with supernatant (SN, 1:2 dilution) obtained from MHEC kept for 24 h in serum-free medium (control), or supernatant obtained from MHEC stimulated for 24 h with 10 ng/mL FGF9; (C) cell size and (D) protein content were determined (n=9). Where indicated, a BMP6 neutralizing antibody or a control antibody (20 μg/mL, each) was added to the supernatants.

Supplemental Figure 1

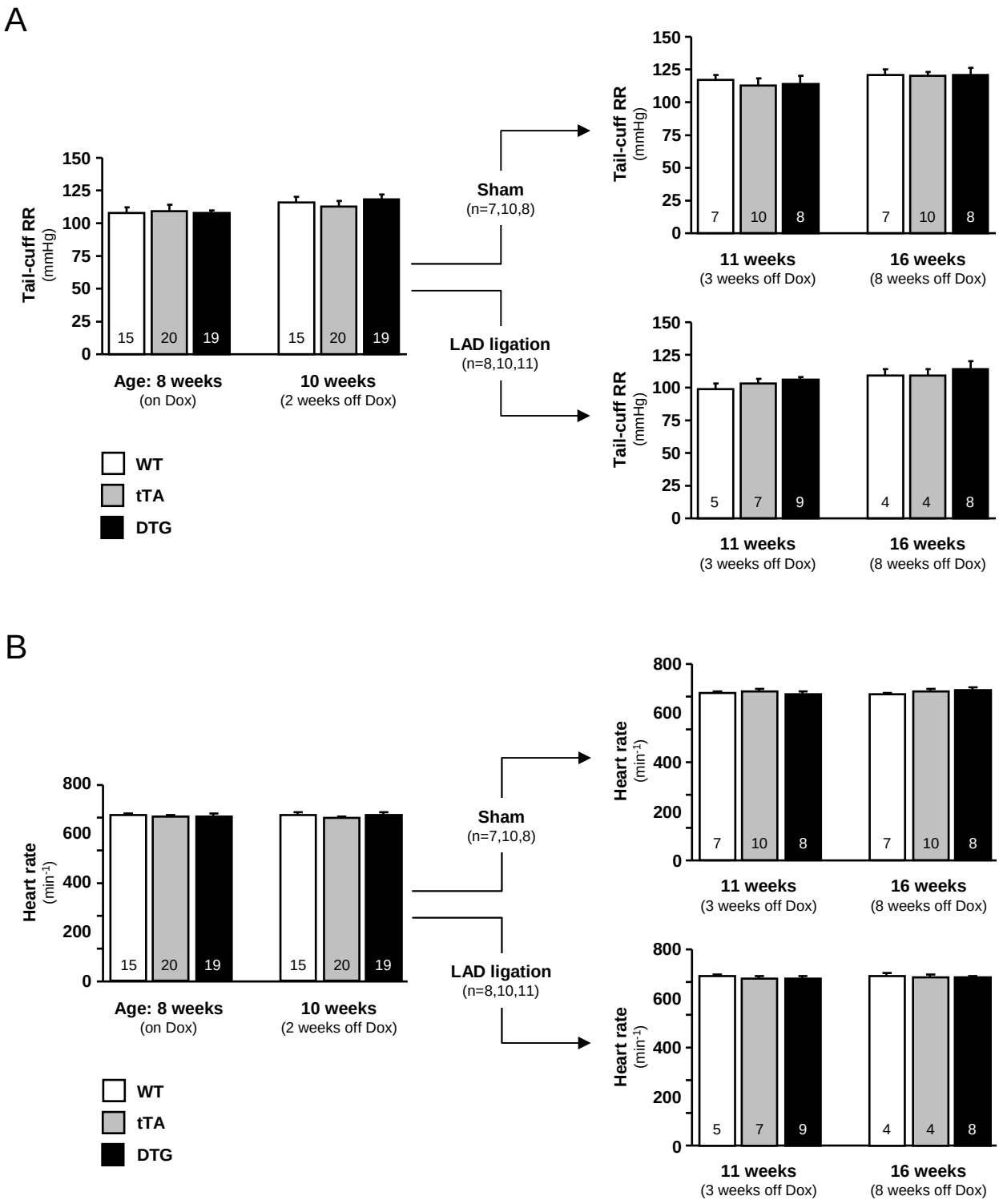

Supplemental Figure 2

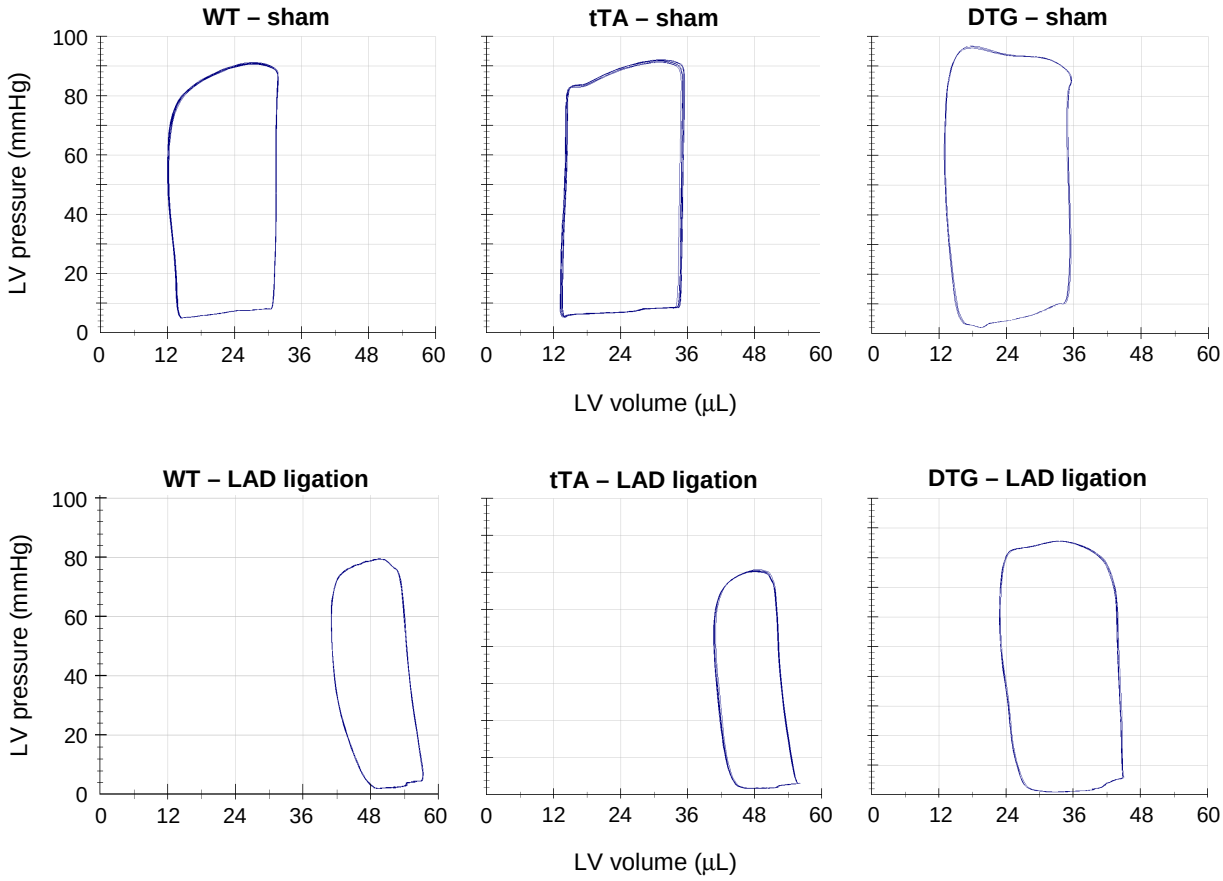

Supplemental Figure 3

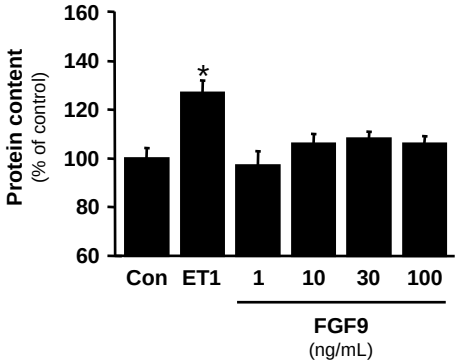

Supplemental Figure 4

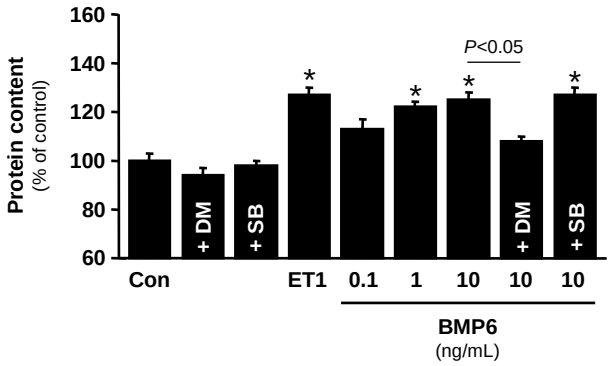

Supplemental Figure 5